

Article

IruO Uses an FAD Semiquinone Intermediate for Iron-Siderophore Reduction

Marek J Kobylarz, Graham A Heieis, Slade A. Loutet, and Michael E. P. Murphy

ACS Chem. Biol., **Just Accepted Manuscript** • Publication Date (Web): 02 May 2017Downloaded from <http://pubs.acs.org> on May 4, 2017**Just Accepted**

“Just Accepted” manuscripts have been peer-reviewed and accepted for publication. They are posted online prior to technical editing, formatting for publication and author proofing. The American Chemical Society provides “Just Accepted” as a free service to the research community to expedite the dissemination of scientific material as soon as possible after acceptance. “Just Accepted” manuscripts appear in full in PDF format accompanied by an HTML abstract. “Just Accepted” manuscripts have been fully peer reviewed, but should not be considered the official version of record. They are accessible to all readers and citable by the Digital Object Identifier (DOI®). “Just Accepted” is an optional service offered to authors. Therefore, the “Just Accepted” Web site may not include all articles that will be published in the journal. After a manuscript is technically edited and formatted, it will be removed from the “Just Accepted” Web site and published as an ASAP article. Note that technical editing may introduce minor changes to the manuscript text and/or graphics which could affect content, and all legal disclaimers and ethical guidelines that apply to the journal pertain. ACS cannot be held responsible for errors or consequences arising from the use of information contained in these “Just Accepted” manuscripts.



1
2
3
4 IruO Uses an FAD Semiquinone Intermediate for Iron-Siderophore Reduction
5
6

7 Marek J. Kobylarz, Graham A. Heieis, Slade A. Loutet, and Michael E.P. Murphy*
8
9
10
11
12
13

14 From: The Department of Microbiology and Immunology, Life Sciences Institute, University of
15

16 British Columbia, Vancouver, British Columbia, V6T 1Z3; Canada
17
18
19
20
21
22

23 *For correspondence

24 Department of Microbiology and Immunology

25 University of British Columbia

26 Vancouver, British Columbia, Canada V6T 1Z3

27 Ph: (604) 822-8022

28 Email: Michael.Murphy@ubc.ca
29
30
31
32
33
34
35
36
37
38
39
40
41
42
43
44
45
46
47
48
49
50
51
52
53
54
55
56
57
58
59
60

Abstract

1
2
3
4
5
6
7 Many pathogenic bacteria including *Staphylococcus aureus* use iron-chelating siderophores to
8 acquire iron. IruO, an FAD-containing NADPH-dependent reductase from *S. aureus*, functions
9 as a reductase for IsdG and IsdI, two paralogous heme degrading enzymes. Also, the gene
10 encoding for IruO was shown to be required for growth of *S. aureus* on hydroxamate
11 siderophores as a sole iron source. Here, we show that IruO binds the hydroxamate-type
12 siderophores desferrioxamine B and ferrichrome A with low micromolar affinity and in the
13 presence of NADPH, Fe(II) was released. Steady-state kinetics of Fe(II) release provides k_{cat}/K_m
14 values in the range of 600 to 7000 $M^{-1}s^{-1}$ for these siderophores supporting a role for IruO as a
15 siderophore reductase in iron utilization. Crystal structures of IruO were solved in two distinct
16 conformational states mediated by the formation of an intramolecular disulfide bond. A putative
17 siderophore binding site was identified adjacent to the FAD cofactor. This site is partly occluded
18 in the oxidized IruO structure consistent with this form being less active than reduced IruO. This
19 reduction in activity could have a physiological role to limit iron release under oxidative stress
20 conditions. Visible spectroscopy of anaerobically reduced IruO showed that the reaction
21 proceeds by a single electron transfer mechanism through an FAD semiquinone intermediate.
22 From the data a model for single electron siderophore reduction by IruO using NADPH is
23 described.
24
25
26
27
28
29
30
31
32
33
34
35
36
37
38
39
40
41
42
43
44
45
46
47
48
49
50
51
52
53
54
55
56
57
58
59
60

1
2
3
4
5
6
7
8
9
10
11
12
13
14
15
Iron is required for growth and the ability to sustain a successful infection by the human pathogen *Staphylococcus aureus*. In *S. aureus*, iron assimilation is critical for many cellular processes, including the tricarboxylic acid cycle.^{1,2} Obtaining iron presents a challenge as most iron is actively sequestered in humans as part of nutritional immunity.^{3,4} For example, hemoglobin is sequestered by haptoglobin, heme by hemopexin and ferric iron (Fe(III)) by transferrin. *S. aureus* uses several iron uptake strategies to obtain iron from the host to satisfy their iron requirements.

16
17
18
19
20
21
22
23
24
25
26
27
28
29
S. aureus can scavenge Fe(III) bound to host proteins using two endogenously synthesized siderophores, staphyloferrin A and staphyloferrin B.⁵ *S. aureus* can also use membrane anchored transporters to obtain iron-bound siderophores produced by other bacteria or fungi. The SstABCD uptake system can internalize catecholate-type siderophores such as enterobactin and petrobactin.⁶ The FhuBGC₂-D2/D1 uptake system can internalize hydroxamate-type siderophores like desferrioxamine B (DFB) and ferrichrome A (FCA).^{7,8} Additionally, *S. aureus* uses the iron-regulated surface determinant (Isd) system to extract heme from hemoglobin, transport it into the cell, and cleave it to release iron.⁹⁻¹²

30
31
32
33
34
35
36
37
38
39
40
41
42
43
44
45
46
47
48
Once internalized, the Fe(III)-siderophore complex must be decoupled to permit iron assimilation into cellular metabolism. One prominent iron release mechanism is a single electron reduction of a chelated Fe(III) complex.¹³ Reduction of Fe(III) to ferrous iron (Fe(II)) greatly decreases the affinity siderophores have for iron ions.¹³ Oxidoreductases have been characterized to reduce Fe(III) complexes, such as the NAD(P)H:flavin oxidoreductase Fre from *Escherichia coli* that can reduce and release flavin adenine dinucleotide (FAD) or flavin mononucleotide (FMN) as free reducing agents.^{14,15} However, most iron-siderophore complexes are reduced by specific siderophore reductases, four of which have been characterized thus far. Both *E. coli* FhuF and *Bacillus halodurans* FchR reduce Fe(III) bound to hydroxamate-type siderophores,^{16,17} *E. coli* YqjH reduces Fe(III) bound to catecholate-type siderophores,¹⁸ and *Thermobifida fusca* FscN reduces Fe(III) bound to fuscachelin.¹⁹

49
50
51
52
53
54
55
56
57
58
59
60
Recently, two reductases associated with iron assimilation have been described in *S. aureus*. First, IruO (iron uptake oxidoreductase) is a FAD-binding, NADPH-dependent reductase capable of donating electrons to either IsdG and IsdI to degrade heme to the staphylobilins and Fe(II).²⁰ Subsequently, bacterial gene deletion studies in *S. aureus* revealed that both IruO and a

1
2
3 predicted nitroreductase (NtrA) are required for heme utilization in *S. aureus* and that IruO and
4 NtrA participate in the utilization of DFB and staphyloferrin A, respectively.²¹
5
6

7 In this study we examined how IruO participates in Fe(III)-siderophore reduction and
8 proposed a mechanism for electron transfer. We demonstrated that IruO specifically reduced the
9 Fe(III)-hydroxamate-type siderophores Fe(III)-DFB and Fe(III)-FCA to release Fe(II) using
10 NADPH as the electron donor. We also solved the X-ray crystal structure of IruO in two distinct
11 conformational states that differ by the formation of an intramolecular disulfide bond. Finally,
12 we showed that under anaerobic conditions, IruO formed a stable FAD semiquinone intermediate
13 to mediate a single electron transfer from the FAD to the Fe(III)-bound siderophore.
14
15
16
17
18
19
20
21
22
23
24
25
26
27
28
29
30
31
32
33
34
35
36
37
38
39
40
41
42
43
44
45
46
47
48
49
50
51
52
53
54
55
56
57
58
59
60

Results

IruO binds and reduces hydroxamate-type siderophores

Recombinant IruO was prepared from *E. coli* under reducing conditions as described previously²⁰ and dialyzed against 50 mM Tris (pH 8.0), 300 mM KCl, and 2 mM TCEP. IruO prepared under reducing conditions is referred to as rdIruO. To assess the activity of rdIruO against hydroxamate-type siderophores, 1 μ M rdIruO was incubated with 100 μ M Fe(III)-DFB and 1 mM ferrozine. Upon the addition of 100 μ M NADPH, an increase in absorption at 562 nm (Fe(II)-ferrozine complex) was observed over 10 minutes, indicating the generation and release of Fe(II) (**Figure 1A**). Omission of either rdIruO or NADPH prevented the production of Fe(II) (**Figures S1A and S1B**). A similar result was observed with 100 μ M Fe(III)-FCA, a structurally distinct hydroxamate siderophore (**Figures 1B, S1C, and S1D**). Unlike Fe(III)-DFB and Fe(III)-FCA, iron-bound ethylenediamine-*N,N'*-bis(2-hydroxyphenylacetic acid) (Fe(III)-EDDHA), a synthetic iron chelator that cannot be used as an iron source by *S. aureus*, could not be reduced by rdIruO (**Figures 1C, S1E and S1F**).

To determine the binding affinity of Fe(III)-DFB and Fe(III)-FCA to rdIruO, tryptophan fluorescence quenching assays were performed. Fluorescence quenching was recorded at various Fe(III)-DFB and Fe(III)-FCA concentrations (0.5 – 20 μ M) with 1 μ M rdIruO. The measured apparent dissociation constant (K_d) of IruO with either siderophore was in the low μ M range (< 3.5 μ M) (**Figure S2**), but was not accurately determined because the rdIruO concentration required to observe fluorescence change was not at least 5-fold lower than the calculated K_d . Nonetheless, the results indicate that IruO can bind two structurally distinct hydroxamate-type siderophores.

Structure of IruO

The crystal structure rdIruO was solved to 1.82 Å resolution with a single molecule in the asymmetric unit. The structure contained the full 344 amino acid sequence with 0.6% of the residues (Val339 and Asn340) categorized as Ramachandran outliers. The rdIruO structure is composed of two distinct domains separated by a hinge region composed of a short, two-stranded antiparallel β -sheet (**Figure 2A**). Based on a Pfam search using the amino acid sequence,²² IruO is classified as a pyridine nucleotide-disulphide oxidoreductase (PNDO),

1
2
3 containing a smaller Rossmann-fold domain that is presumed to bind NAD(P)H (residues 121 -
4 244) and a second, larger PNDO domain that binds FAD. In the structure, the latter domain is
5 assembled from the N-terminal and C-terminal ends of the polypeptide chain (residues 1 - 120,
6 and 245 – 316). The PNDO domain also contained a dimerization interface formed when a
7 rdIruO dimer is constructed by applying crystallographic symmetry (**Figure 2B**). The buried
8 surface at this interface is $\sim 2600 \text{ \AA}^2$ as quantified by PISA.²³ Part of the interface is composed of
9 a 28-residue C-terminal α -helix projecting from the PNDO domain (**Figures 2A and 2B**). To
10 show that dimerization occurred in solution the mass of rdIruO was measured by size exclusion
11 chromatography with multi-angle light scattering (SEC-MALS) to be 77 kDa (**Figure S3A**),
12 similar to the predicted dimeric mass of 76.4 kDa.
13
14
15
16
17
18
19
20

21 Buried within the PNDO domain is a single FAD cofactor modeled at full occupancy
22 (**Figure 2C**). The FAD is oriented such that the *re*-face of the isoalloxazine ring is exposed to the
23 solvent and the adenosine and ribitol moieties formed multiple hydrogen bonds with water
24 molecules and residues of the PNDO domain (**Figure 2C**). The isoalloxazine ring is stabilized
25 within the PNDO domain by Tyr43 through π - π stacking at the *si*-face and Val324 through an
26 intermolecular hydrophobic interaction at the *re*-face (**Figure 2C**). Val324 is part of the
27 C-terminal α -helix and interacted with the FAD isoalloxazine ring in the adjacent subunit
28 (**Figure 2C**). A shallow pocket located next to the *re*-face of the isoalloxazine ring is constructed
29 from residues located in the PNDO domain, NADPH domain, hinge region and the C-terminal
30 helix from the adjacent subunit (**Figures 2D and S4A**). The pocket is primarily composed of
31 polar and positively charged residues such as Lys39, Thr159, Arg247, His294, Tyr323 and
32 His327 (**Figure S4A**). In the rdIruO structure a glycerol molecule, used as a cryoprotectant, is
33 observed bound in the pocket adjacent to the FAD cofactor. The proximity of the pocket to the
34 cofactor and the polar nature of the residues lining the pocket suggested this is a putative
35 siderophore binding site.
36
37
38
39
40
41
42
43
44
45
46
47
48
49

50 *IruO mediates electron transfer from NADPH to Fe(III)-siderophores complexes via an FAD*
51 *neutral semiquinone intermediate*
52

53 An anaerobic environment was used to investigate the rdIruO electron transfer
54 mechanism. UV-visible spectroscopy revealed that the FAD cofactor of rdIruO was in the
55 oxidized state (FAD_{ox}) as characterized by the peaks at 376 and 464 nm (**Figure 3A**). Upon the
56
57
58
59
60

1
2
3 addition of equimolar NADPH, spectra corresponded to the neutral semiquinone state (FAD_{sq}) as
4 evidenced by a decrease in the peaks at 376 and 464 nm and a subsequent increase in a broad
5 peak between 550-650 nm (**Figure 3B**).²⁴ To examine if additional NADPH resulted in full
6 reduction of FAD to the hydroquinone state (FAD_{hq}) in rdIruO 5-fold excess of NADPH was
7 added to rdIruO and spectra were recorded after 5 min. The FAD was only reduced to the neutral
8 FAD_{sq} state and not the FAD_{hq} state (**Figure S5A**). Unlike rdIruO, thioredoxin reductase
9 (NWMN_0732), the closest homolog to IruO in *S. aureus*, did not form the FAD_{sq} state; instead,
10 formed the fully reduced FAD_{hq} state in the presence of 150 μM NADPH (**Figure S5B**). The
11 FAD_{hq} state in rdIruO was attained by the addition of 100 μM sodium dithionite (**Figure 3C**).

12
13
14
15
16
17
18
19
20
21
22
23
24
25
26
27
28
29
30
31
32
33
34
35
36
37
38
39
40
41
42
43
44
45
46
47
48
49
50
51
52
53
54
55
56
57
58
59
60
Oxidation of NADPH to NADP^+ is a two-electron process, yet the FAD cofactor in
rdIruO only accepted one electron to form FAD_{sq} . Therefore, we hypothesized that NADPH
transfers the second electron through the interacting PNDO domains to the second FAD cofactor
in the adjacent subunit. A titration of rdIruO with NADPH resulted in formation of the FAD_{sq} at
a molar ratio of 0.5 NADPH to rdIruO (**Figure 3D**). Further additions of NADPH did not yield
further reduction of FAD_{sq} . Next, we hypothesized that the FAD_{sq} from rdIruO is able to reduce
Fe(III)-siderophore complexes. Indeed, addition of Fe(III)-DFB to rdIruO FAD_{sq} resulted in a
loss of the broad peak between 550-650 nm (**Figure 3E**). When Ga(III)-DFB, a non-reducible
iron analog, was added to rdIruO FAD_{sq} , no spectral changes were observed (**Figure 3F**).
Overall, the data indicates that rdIruO mediated the transfer of two electrons from one NADPH
to reduce two Fe(III)-DFB molecules via a FAD_{sq} intermediate.

An intramolecular disulfide bond can form in IruO

IruO was subjected to a molar excess of potassium ferricyanide to form oxidized IruO
(oxIruO). Potassium ferricyanide was used because it is a mild oxidizing agent. The oxIruO
crystal structure was solved to 2.3 Å resolution. A structural overlay between rdIruO and oxIruO
revealed that the NADPH domain of the oxIruO structure rotated $\sim 90^\circ$ with respect to the PNDO
domain (**Figures 4A and 4B**). A disulfide bond was observed between Cys248 and Cys265,
along with disruption of the structure of the hinge region (**Figure 4C**). In rdIruO, Cys248 is
located within the hinge region and Cys265 is located in a surface loop of the PNDO domain.
The conformation of the PNDO and NADPH domains in the oxIruO structure are largely
unchanged from the domains in the rdIruO structure (RMSD over all $\text{C}\alpha < 0.5$ Å). However, the

1
2
3
4
5
6
7
8
9
10
11
12
13
14
15
16
17
18
19
20
21
22
23
24
25
26
27
28
29
30
31
32
33
34
35
36
37
38
39
40
41
42
43
44
45
46
47
48
49
50
51
52
53
54
55
56
57
58
59
60

90° twist of the NADPH domain resulted in a significant conformational change in the putative siderophore binding site. Compared to the rdIruO structure, the putative siderophore binding site in the oxIruO structure was narrower (**Figure 4D**). The volume of the putative binding groove decreased from 1233 Å³ to 997 Å³ as measured using the program 3V (**Figure S6**).²⁵ Similar to rdIruO, oxIruO was also dimeric in solution with a mass of 74 kDa as measured by SEC-MALS (**Figure S3B**). A DTNB assay detected ~1.7 thiol (SH) groups per rdIruO subunit compared to ~0.2 SH groups per oxIruO subunit suggesting that a disulfide bond was formed in solution as was observed in the oxIruO structure.

To determine how disulfide bond formation affects the function of IruO, the ferrozine assay was used to determine steady-state kinetic parameters from reactions of either rdIruO or oxIruO against varying concentrations of Fe(III)-DFB, Fe(III)-FCA and NADPH (**Table 1 and Figures S7 and S8**). Both oxidized and reduced IruO displayed Michaelis-Menten kinetics over the conditions tested. The oxidation of IruO resulted in a reduction of the enzymatic efficiency (k_{cat}/K_m) for both Fe(III)-DFB and Fe(III)-FCA by ~5-fold. However, the observed K_m was negligibly impacted by the disulfide bond formation, except for oxIruO with Fe(III)-FCA, which was 5-fold higher. A consistent, distinguishable difference in the k_{cat}/K_m (~2-fold) was evident between Fe(III)-DFB and Fe(III)-FCA with either rdIruO or oxIruO, indicating that structural differences between the siderophores impact iron reduction. For NADPH, the k_{cat}/K_m was comparable, suggesting that the oxidation of IruO does not impact NADPH utilization; an observation supported by the minimal conformational changes observed in the putative NADPH binding sites between the oxIruO and rdIruO structures. Overall, the oxidation of IruO and formation of an intramolecular disulfide bond resulted in a defect in IruO Fe(III)-siderophore reductase activity *in vitro*. Future studies are required to validate the role cysteine oxidation has on regulating IruO activity *in vivo*.

Reduced IruO is the preferred form of IruO for heme degradation by IsdI

IsdI-heme degradation reactions with rdIruO and NADPH (**Figure S9A**) were faster than those with oxIruO and NADPH (**Figure S9B**) as judged by the decreasing height of the Soret peak at 412 nm. The second peak at 240 nm corresponds to the presence of NADPH in the assay. Heme degradation rates observed under these conditions were calculated to be $0.39 \pm 0.02 \text{ min}^{-1}$ and $0.13 \pm 0.005 \text{ min}^{-1}$ for rdIruO and oxIruO, respectively. Similar to activity in the presence of

1
2
3 hydroxymate siderophores, the introduction of an intramolecular disulfide bond decreased IruO
4 activity.
5
6
7
8
9
10
11
12
13
14
15
16
17
18
19
20
21
22
23
24
25
26
27
28
29
30
31
32
33
34
35
36
37
38
39
40
41
42
43
44
45
46
47
48
49
50
51
52
53
54
55
56
57
58
59
60

Discussion

The few siderophore reductases characterized in the literature are of two types: iron-sulfur cluster (FeS) cofactor-containing reductases and FAD cofactor-containing reductases. *E. coli* contains both types of reductases, FhuF (FeS type),¹⁷ and YqjH (FAD type),¹⁸ which were shown to reduce hydroxamate-type and catecholate-type siderophores, respectively. A FeS-containing reductase (FchR) in *B. halodurans* was characterized that reduces both Fe(III)-dicitrate and hydroxamate-type siderophores like Fe(III)-schizokinen.¹⁶ *T. fusca* FscN is an FAD-containing enzyme of the YqjH family that reduces Fe(III)-fuschachelin, a mixed catecholate/hydroxamate siderophore.¹⁹ Additionally, several IruO homologs have been identified by sequence analysis in Gram-positive bacteria that include *Bacillus subtilis*, *Bacillus anthracis*, and *Listeria monocytogenes*.²⁰ The gene of the *L. monocytogenes* homolog (LMO1961) appears to be part of a larger gene cluster predicted to encode for hydroxamate-type siderophore import machinery.²⁶

In addition to IruO, *S. aureus* contains a gene annotated as a flavin-containing reductase, NtrA, that is involved in iron utilization from Fe(III)-SA.²¹ Under iron restriction, *S. aureus* alters its metabolism to conserve iron by inducing the “iron sparing” response, which results in the down-regulation of the tricarboxylic acid cycle and up-regulation of glycolysis.¹ Coupled with the recent discovery that *S. aureus* produces staphyloferrin B without the need of the iron-requiring tricarboxylic acid cycle,²⁷ our data suggests further adaptation to utilize flavoproteins for iron assimilation as a strategy to conserve iron.

IruO utilizes a single electron transfer mechanism to reduce Fe(III)-bound hydroxamate-type siderophores. IruO performs a unique, single electron transfer mechanism where electrons are transferred from NADPH to FAD and then from FAD to its siderophore substrate (**Scheme 1**). In this proposed mechanism, NADPH could bind to either or both NADPH-binding domains in the IruO dimer complex, but only one NADPH substrate can donate an electron to each of the FAD cofactors present in the IruO dimer complex. The NADPH bound to the other protomer is proposed to remain in a primed state to donate two electrons once the enzyme has completely turned over. Furthermore, based on the orientation of the NADPH-binding domain and FAD-binding domain (**Figure S4D**), a conformational change is likely to be required to bring the NADPH and FAD molecules into close proximity to initiate electron transfer. The FAD cofactor in IruO is reduced to a stable neutral semiquinone state instead of the fully reduced

1
2
3 hydroquinone state. Under the conditions examined, FAD_{sq} is the most likely physiologically
4 relevant intermediate used for Fe(III)-DFB and Fe(III)-FCA iron reduction (**Scheme 1**). Since
5 NADPH must donate two electrons simultaneously and a single subunit of IruO can only accept
6 one electron, we propose that the second electron is directly transferred through the PNDO
7 domain's dimeric interface to the second FAD cofactor (**Scheme 1**). This mechanism is in
8 marked contrast to those proposed for YqjH and FscN.^{18,19} In the YqjH reaction cycle, two
9 Fe(III)-siderophores are reduced in a NAD(P)H-dependent, sequential manner by performing
10 two single electron transfer reactions. First, one electron from the fully reduced FAD_{hq}
11 intermediate is transferred to a Fe(III)-siderophore followed by a second one electron transfer
12 from the FAD_{sq} intermediate to a second Fe(III)-siderophore.¹⁸

21 Fe(III)-siderophore reduction is a common mechanism to decrease the affinity
22 siderophores have for the bound iron atom. Reduction potentials vary widely across the three
23 major classes of siderophores with catecholate-type siderophores possessing the lowest E'_0 , pH
24 7.0 values at approximately -750 mV, hydroxamate-type siderophores at approximately -300 mV
25 and carboxylate-type siderophores at approximately -100 mV.¹³ In this study, Fe(III)-FCA (-400
26 mV (pH 7.0)), Fe(III)-DFB (-468 mV (pH 7.0)) and EDDHA (-560 mV (pH 7.4)) were used to
27 characterize IruO activity.²⁸ Under reducing conditions, IruO was more active against Fe(III)-
28 FCA compared to Fe(III)-DFB (**Table1**), which correlates to their respective reduction
29 potentials. The significantly lower potential for Fe(III)-EDDHA could be outside the effective
30 range for an IruO reduction-oxidation reaction and thus could explain why IruO was not active
31 against Fe(III)-EDDHA.

41 IruO represents the first solved structure of a validated Fe(III)-siderophore reductase. A
42 search of the Protein Data Bank using the Dali Server revealed that the top three homologs
43 (RMSD ≥ 5 Å) include ferredoxin-NADP⁺ oxidoreductases (FNR) from *B. subtilis*,²⁹ and
44 *Chlorobaculum tepidum*,³⁰ and a thioredoxin reductase-like protein from *Thermus thermophiles*
45 (PDBID: 2ZBW), all of which contain an FAD cofactor.³¹ A sequence alignment between IruO
46 and all three homologs revealed a core set of conserved residues within the PNDO domain
47 responsible for binding the isoalloxazine ring with the exception of one variable residue that
48 interacted with the *re*-face of the isoalloxazine ring. A putative NADPH binding site in IruO was
49 located exclusively along a shallow groove in the NADPH domain based on a structural overlay
50 with FNR from *B. subtilis* (PDBID: 3LZW) (**Figures S4B and S4C**).²⁹ The NADPH binding
51
52
53
54
55
56
57
58
59
60

1
2
3 domains overlay with an RMSD of 0.73 Å over 93 C α atoms; however, the NADPH binding
4 residues are poorly conserved suggesting that IruO binds NADPH in a different configuration. A
5 conformational change upon NADP⁺ binding may account for the differences observed in the
6 NADPH binding pockets. IruO is homologous with thioredoxin reductases, which are
7 responsible for reducing disulfide bonds in thioredoxins.³² In *S. aureus* strain Newman, the
8 closest homolog to IruO is TrxB (NWMN_0732) with a sequence identity of 24%. Superposition
9 of the structure of TrxB (PDBID: 4GCM) with rdIruO revealed a conserved overall fold with a
10 RMSD value of ~3.5 Å over 231 C α atoms; however, the residues in the FAD binding site are
11 poorly conserved (**Figure S10**). The isoalloxazine ring in rdIruO is partially exposed to the
12 solvent whereas the isoalloxazine ring in TrxB is blocked at the *re*-face by a redox active
13 disulfide bond that is essential for electron transfer to thioredoxin.
14
15
16
17
18
19
20
21
22

23 IruO bound Fe(III)-FCA, Fe(III)-DFB and NADPH models were generated using
24 AutoDock Vina (**Figure S11**).³³ Substrate binding models were generated using the rdIruO
25 crystal structure in its dimeric form. The model showed NADPH bound into its predicted binding
26 groove located along the surface of the NADPH-domain (**Figures S11A and S11B**). Based on
27 the model, the C4 atom within the nicotinamide ring of NADPH was ~16 Å away from the FAD
28 cofactor, which indicates that a conformational change most likely occurs to allow electron
29 transfer between NADPH and FAD. Additionally, both Fe(III)-DFB and Fe(III)-FCA bound into
30 the predicted rdIruO active site and in close proximity to the FAD cofactor (**Figures S11C-F**).
31 The Fe(III) bound in each siderophore was approximately ~7-8 Å away from the FAD cofactor.
32 Both Fe(III)-FCA and Fe(III)-DFB were observed to interact with residues present in the PNDO
33 domain and C-terminal α -helix from the adjacent subunit (**Figures S11D and S11F**). A sharing
34 of the active site between IruO subunits for siderophore binding further highlights the
35 importance of the dimeric state in IruO,
36
37
38
39
40
41
42
43
44
45

46 IruO forms an intramolecular disulfide bond, which significantly altered the relative
47 orientation of the PNDO and NADPH domains and negatively impacted siderophore reduction
48 activity *in vitro*. Heme degradation by IsdI was also impaired when using oxIruO as the electron
49 donor. Previous microarray studies show that oxidative and nitrosative stress results in the
50 dysregulation of iron-homeostasis in *S. aureus* leading to the up-regulation of most iron uptake
51 systems.^{34,35} An excess of free iron could increase the generation of reactive oxygen species that
52 are responsible for biomolecule damage. Thus, a redox sensitive, reversible disulfide bond in
53
54
55
56
57
58
59
60

1
2
3 IruO may function to regulate the amount of iron being released from siderophores under
4 oxidative conditions. Interestingly, the siderophore reductase FhuF in *E. coli* is repressed by the
5 oxidative response regulator, OxyR.³⁶ OxyR itself is regulated by redox sensitive cysteines that
6 form an intramolecular disulfide bond upon H₂O₂ exposure.³⁷ Disulfide bond formation induces
7 a conformational change that activates OxyR to bind DNA and regulate the transcription of
8 several genes such as *katG* (hydrogen peroxidase I), *gorA* (glutathione reductase) and *fhuF*
9 (siderophore reductase).³⁶ Future studies are required to validate the existence of the
10 intramolecular disulfide bond in IruO *in vivo* under oxidizing conditions and to determine if IruO
11 activity is altered by oxidative stress effectors.
12
13
14
15
16
17
18
19
20
21
22
23
24
25
26
27
28
29
30
31
32
33
34
35
36
37
38
39
40
41
42
43
44
45
46
47
48
49
50
51
52
53
54
55
56
57
58
59
60

Methods

Cloning and protein expression of IruO

Recombinant rdIruO and NWMN0732 were expressed from *E. coli* and purified as previously described.²⁰ Selenomethionine (SeMet) labelled rdIruO (SeIruO) was produced as described.³⁸ oxIruO was purified by exposing cell lysates to 2 M potassium ferricyanide for approximately 30 minutes and omitting Tris(2-carboxyethyl)phosphine (TCEP) from all purification steps. All protein samples were concentrated to 20 mg/mL in 50 mM Tris pH 8.0, 300 mM KCl. TCEP was only included for rdIruO. Protein quality was assayed by SDS-PAGE gel, which showed >95% purity.

IruO structure determination

Crystals of IruO were obtained by sitting drop vapour diffusion at 4 °C. SeIruO and rdIruO drops contained 2 µL of 20 mg/mL protein and 2 µL of 0.2 M magnesium acetate and 8-11% PEG 3350. Crystals were further optimized by seeding drops with 0.4 µL crushed crystals, which was initially prepared by crushing ~2 small crystals in 10 µL mother liquor from the originating crystal condition and diluted to 10^{-4} - 10^{-5} in the same mother liquor. OxIruO drops contained 2 µL protein solution and 2 µL 2.0-3.0 M sodium formate pH 7.0 and were further optimized by streak seeding with a cat whisker through a drop with ~2 crushed crystals in 10 µL from the originating mother liquor. All crystals were soaked for <30 s in mother liquor supplemented with 30 % glycerol and flash frozen in liquid nitrogen.

Single wavelength anomalous diffraction data for SeIruO was collected from a single crystal at a wavelength of 0.979383 Å on beamline 7-1 at the Stanford Synchrotron Radiation Light Source. SeIruO crystals grew in the space group *C2* with one IruO molecule in the asymmetric unit. Data was integrated and scaled using XDS.³⁹ Phase determination and model building were performed using AutoSol and Autobuild programs from Phenix.⁴⁰ The initial figure of merit from AutoSol was 0.46 and AutoBuild built 299 of 344 residues. The structure was manually edited using Coot,⁴¹ and refinement was performed with Phenix.refine.⁴⁰ Diffraction data from a native rdIruO crystal was collected at a wavelength of 0.976240 Å on beamline 08B1 at the Canadian Light Source. Data was integrated and scaled in space group *C2* using Mosflm and SCALA from CCP4.^{42,43} The structure was solved by molecular replacement

1
2
3 using the coordinates of SeMet-labeled IruO as the search model in Phenix.phaser.⁴⁰ A crystal of
4 native oxIruO was collected at a wavelength of 0.975302 Å on beamline 7-1 at the Stanford
5 Synchrotron Radiation Light Source. Native oxIruO crystals grew in the space group $P4_12_12$.
6 The data was integrated and scaled using XDS.³⁹ The structure was solved by molecular
7 replacement similarly to native rdIruO with the exception that the search model was separated
8 into three fragments (residues 1-120, 126-240 and 249-344). The structures were manually edited
9 using Coot,⁴¹ and refinement was performed with Phenix.refine⁴⁰ using TLS refinement with 3
10 TLS groups (residues 1-132, 133-246 and 247-344). Data collection and refinement statistics are
11 provided in **Table S1**.
12
13
14
15
16
17
18
19

20 21 *Determination of oligomeric state in solution*

22 Samples of rdIruO and oxIruO were analyzed by SEC-MALS. Protein samples were
23 concentrated to 2 mg/mL in 50 mM Tris pH 8.0, 300 mM KCl and 100 μL was injected into a
24 HPLC 1260 Infinity LC (Agilent Technologies) attached to a Superdex 200 5/150 column (GE
25 Healthcare) with a flow rate of 0.2 mL/min. Data were collected using a miniDAWN TREOS
26 multi-angle static light scattering device and an Optilab T-rEX refractive index detector (Wyatt
27 Technologies). Analysis was performed using the ASTRA6 program (Wyatt Technologies).
28
29
30
31
32
33
34

35 *Assay of IruO sulfhydryls*

36 Sulfhydryls on rdIruO and oxIruO were quantified using a DTNB method as previously
37 described.⁴⁴
38
39
40
41

42 *Detection of FAD_{sq} by anaerobic UV-visible absorption spectroscopy*

43 Room temperature UV-visible absorption spectra (300-800 nm) were measured with a Nanodrop
44 2000c spectrophotometer (Thermo Scientific) in an anaerobic chamber (Belle Technology). All
45 reagents were transferred into the chamber and allowed to equilibrate overnight with a maximum
46 O₂ level of ~10 ppm. Sodium dithionite (Sigma) was prepared fresh in the anaerobic chamber
47 and used immediately. Samples of rdIruO (30 μM) in 50 mM sodium phosphate buffer, pH 7.4
48 were used for all assays. Upon the addition of 20 or 150 μM NADPH (Calbiochem) or 100 μM
49 sodium dithionite, spectra were recorded every 30 s for 5 minutes. To demonstrate electron
50 transfer from the IruO FAD_{sq} to siderophores, 10 μM of NADPH was added to IruO and
51
52
53
54
55
56
57
58
59
60

1
2
3 incubated for 5 minutes. Next, 60 μM of Fe(III)-DFB was added to the mixture and the spectra
4 were recorded as above. Negative controls were NWMN_0732 in place of IruO and Ga(III)-DFB
5 in place of Fe(III)-DFB. Fe(III)-DFB and Ga(III)-DFB were prepared in advance by adding
6 together FeCl_3 , or $\text{Ga}(\text{NO}_3)_3$ and apo-DFB (Sigma) in a 1:1 molar ratio and incubating at room
7 temperature for one hour.
8
9

10
11
12 To determine the molar ratio of NADPH required to form the FAD semiquinone, 30 μM
13 of rdIruO was titrated with 5 μM NADPH aliquots from a 5 mM working stock. After each
14 NADPH addition, the mixture was allowed to incubate for 5 minutes and then spectra were
15 recorded at 600 nm to detect the formation of the FAD semiquinone. The NADPH titration
16 experiment was repeated in triplicate.
17
18
19
20
21

22 *IruO affinity for siderophores by fluorescence spectroscopy*

23
24 Quenching of internal tryptophan fluorescence of IruO was measured using a Cary Eclipse
25 fluorescence spectrophotometer at 25 °C. 1 μM rdIruO, in 50 mM sodium phosphate, pH 7.4,
26 were titrated with 0.5 - 20 μM of Fe(III)-DFB or Fe(III)-FCA. Fe(III)-FCA was prepared in an
27 identical manner to Fe(III)-DFB as described in the section above. The excitation and emission
28 slits were 10 nm and the detector voltage was 900 V. Samples were excited at 292 nm and
29 emission spectra (310-380 nm) were measured. Emission at 350 nm was selected for analysis.
30 Each replicate is the average intensity of three sequential scans and this was performed in
31 triplicate. Apparent dissociation constants (K_d) were determined by fitting data to a one-site
32 binding model.
33
34
35
36
37
38
39
40
41

42 *IruO enzyme kinetics*

43
44 A ferrozine-based assay was used to measure the generation of Fe(II) as previously described.⁴⁵
45 500 μL reaction mixtures contained 1 μM rdIruO, 1 mM ferrozine, 100 μM NADPH and 100
46 μM Fe(III)-siderophore in 50 mM sodium phosphate buffer (pH 7.4) at room temperature.
47 Absorption spectra of the reaction mixtures from 400 to 800 nm were monitored every 30
48 seconds for 10 minutes. The ferrozine-Fe(II) complex was detected at 562 nm using an
49 extinction coefficient of 27900 $\text{M}^{-1}\text{cm}^{-1}$.⁴⁵ To determine kinetic parameters, 500 μL reactions
50 were prepared with 50 mM sodium phosphate buffer (pH 7.4), 1 - 60 μM of NADPH, 1 mM
51 ferrozine, 1 - 250 μM and Fe(III)-DFB or Fe(III)-FCA. 0.3 μM oxIruO was used in reactions for
52
53
54
55
56
57
58
59
60

1
2
3 both siderophores and 0.1 μM and 0.02 μM rdIruO was used for Fe(III)-DFB and Fe(III)-FCA,
4 respectively. Data was collected in triplicate on a Varian Cary 60 UV-Vis spectrophotometer at a
5 temperature of 25 $^{\circ}\text{C}$. Data were fit by non-linear regression and with a least-squares fit to
6 Michaelis-Menten kinetics model.
7
8
9

10 11 12 *Heme degradation assays*

13
14 IsdI was reconstituted with heme as previously described.⁴⁶ Heme degradation was initiated with
15 1 μM oxIruO or rdIruO and 200 μM NADPH in the presence of 500 μM catalase and 4 U/mL
16 superoxide dismutase. Spectra of the reaction mixtures from 300 to 700 nm were monitored
17 every minute for twenty minutes or the absorbance at the Soret peak (412 nm) was measured
18 every 0.1 second for 60 seconds. To calculate reaction rates the absorbance at the Soret peak was
19 converted to the concentration of IsdI-heme based on the published extinction coefficient (126
20 $\text{mM}^{-1} \text{cm}^{-1}$).⁴⁷ Linear regressions were calculated from data taken between 10 and 60 seconds
21 after initiation of the reaction and the slope of the lines were taken as the reaction rates.
22 Reactions were done in triplicate and data presented in the text are the means and standard errors
23 of the mean. Linear regression R^2 -values were all above 0.97 and all slopes significantly deviated
24 from a value of zero ($p < 0.0001$).
25
26
27
28
29
30
31
32
33

34 35 *Software*

36
37 All kinetic calculations and statistical analyses were performed using GraphPad Prism 6.00/7.00.
38
39
40
41
42
43

44 45 **Acknowledgments**

46 This research is supported by Canadian Institutes of Health Research grant MOP-102596 to M.
47 Murphy. G. Heieis was supported by a University of British Columbia Science Undergraduate
48 Research Experience award. S. Loutet was supported by a Natural Sciences and Engineering
49 Research Council of Canada Post-Doctoral Fellowship. We would like to thank F. Rosell for
50 assistance with the fluorescence spectrophotometer and A. Arrieta for technical assistance.
51
52
53
54

55 Use of the Stanford Synchrotron Radiation Lightsource, SLAC National Accelerator
56 Laboratory, is supported by the U.S. Department of Energy, Office of Science, Office of Basic
57
58
59
60

1
2
3 Energy Sciences under Contract No. DE-AC02-76SF00515. The SSRL Structural Molecular
4 Biology Program is supported by the DOE Office of Biological and Environmental Research,
5 and by the National Institutes of Health, National Institute of General Medical Sciences
6 (including P41GM103393). The contents of this publication are solely the responsibility of the
7 authors and do not necessarily represent the official views of NIGMS or NIH.
8
9

10
11 Research described in this paper was performed using beamline 08B1-1 at the Canadian
12 Light Source, which is supported by the Natural Sciences and Engineering Research Council of
13 Canada, the National Research Council Canada, the Canadian Institutes of Health Research, the
14 Province of Saskatchewan, Western Economic Diversification Canada, and the University of
15 Saskatchewan.
16
17
18
19
20
21

22
23 **Supporting Information:** Table showing X-ray diffraction data collection and refinement
24 statistics. Figures showing iron reduction from hydroxamate-type siderophores is rdIruO- and
25 NADPH-dependent, rdIruO binds hydroxamate-type siderophores, IruO forms a dimer in
26 solution, rdIruO substrate binding sites, rdIruO and NWMN_0732 differentially reduce FAD
27 upon NADPH exposure, oxIruO putative siderophore binding site volume is smaller compared to
28 rdIruO, steady-state kinetics of IruO with Fe(III)-DFB and Fe(III)-FCA, steady-state kinetics of
29 IruO with NADPH, rdIruO is the preferred form of IruO from heme degradation, IruO FAD
30 binding and active site formation is divergent from TrxB, and rdIruO dimer modeled with
31 NADPH, Fe(III)-DFB and Fe(III)-FCA. (LINK TO SUPPORTING INFORMATION)
32
33
34
35
36
37
38
39
40
41
42
43
44
45
46
47
48
49
50
51
52
53
54
55
56
57
58
59
60

References

- (1) Friedman, D. B., Stauff, D. L., Pishchany, G., Whitwell, C. W., Torres, V. J., and Skaar, E. P. (2006) *Staphylococcus aureus* redirects central metabolism to increase iron availability. *PLoS Pathog.* **2**, e87.
- (2) Andrews, S. C., Robinson, A. K., and Rodriguez-Quinones, F. (2003) Bacterial iron homeostasis. *FEMS Microbiol. Rev.* **27**, 215-237.
- (3) Cassat, J. E., and Skaar, E. P. (2013) Iron in infection and immunity. *Cell Host Microbe* **13**, 509-519.
- (4) Weinberg, E. D. (1974) Iron and susceptibility to infectious disease. *Science* **184**, 952-956.
- (5) Beasley, F. C., and Heinrichs, D. E. (2010) Siderophore-mediated iron acquisition in the staphylococci. *J. Inorg. Biochem.* **104**, 282-288.
- (6) Beasley, F. C., Marolda, C. L., Cheung, J., Buac, S., and Heinrichs, D. E. (2011) *Staphylococcus aureus* transporters Hts, Sir, and Sst capture iron liberated from human transferrin by staphyloferrin A, staphyloferrin B, and catecholamine stress hormones, respectively, and contribute to virulence. *Infect. Immun.* **79**, 2345-2355.
- (7) Sebulsky, M. T., Hohnstein, D., Hunter, M. D., and Heinrichs, D. E. (2000) Identification and characterization of a membrane permease involved in iron-hydroxamate transport in *Staphylococcus aureus*. *J. Bacteriol.* **182**, 4394-4400.
- (8) Sebulsky, M. T., and Heinrichs, D. E. (2001) Identification and characterization of fhuD1 and fhuD2, two genes involved in iron-hydroxamate uptake in *Staphylococcus aureus*. *J. Bacteriol.* **183**, 4994-5000.
- (9) Skaar, E. P., and Schneewind, O. (2004) Iron-regulated surface determinants (Isd) of *Staphylococcus aureus*: stealing iron from heme. *Microbes Infect.* **6**, 390-397.
- (10) Grigg, J. C., Ukpabi, G., Gaudin, C. F., and Murphy, M. E. (2010) Structural biology of heme binding in the *Staphylococcus aureus* Isd system. *J. Inorg. Biochem.* **104**, 341-348.
- (11) Mazmanian, S. K., Skaar, E. P., Gaspar, A. H., Humayun, M., Gornicki, P., Jelenska, J., Joachimiak, A., Missiakas, D. M., and Schneewind, O. (2003) Passage of heme-iron across the envelope of *Staphylococcus aureus*. *Science* **299**, 906-909.
- (12) Wu, R., Skaar, E. P., Zhang, R., Joachimiak, G., Gornicki, P., Schneewind, O., and Joachimiak, A. (2005) *Staphylococcus aureus* IsdG and IsdI, heme-degrading enzymes with structural similarity to monooxygenases. *J. Biol. Chem.* **280**, 2840-2846.
- (13) Hider, R. C., and Kong, X. (2010) Chemistry and biology of siderophores. *Nat. Prod. Rep.* **27**, 637-657.
- (14) Ingelman, M., Ramaswamy, S., Niviere, V., Fontecave, M., and Eklund, H. (1999) Crystal structure of NAD(P)H:flavin oxidoreductase from *Escherichia coli*. *Biochemistry* **38**, 7040-7049.
- (15) Fontecave, M., Coves, J., and Pierre, J. L. (1994) Ferric reductases or flavin reductases? *Biometals* **7**, 3-8.
- (16) Miethke, M., Pierik, A. J., Peuckert, F., Seubert, A., and Marahiel, M. A. (2011) Identification and characterization of a novel-type ferric siderophore reductase from a Gram-positive extremophile. *J. Biol. Chem.* **286**, 2245-2260.
- (17) Matzanke, B. F., Anemuller, S., Schunemann, V., Trautwein, A. X., and Hantke, K. (2004) FhuF, part of a siderophore-reductase system. *Biochemistry* **43**, 1386-1392.
- (18) Miethke, M., Hou, J., and Marahiel, M. A. (2011) The siderophore-interacting protein YqjH acts as a ferric reductase in different iron assimilation pathways of *Escherichia coli*. *Biochemistry* **50**, 10951-10964.
- (19) Li, K., Chen, W. H., and Bruner, S. D. (2015) Structure and mechanism of the siderophore-interacting protein from the fuscachelin gene cluster of *Thermobifida fusca*. *Biochemistry* **54**, 3989-4000.
- (20) Loutet, S. A., Kobylarz, M. J., Chau, C. H., and Murphy, M. E. (2013) IruO is a reductase for heme degradation by IsdI and IsdG proteins in *Staphylococcus aureus*. *J. Biol. Chem.* **288**, 25749-25759.

- 1
2
3
4 (21) Hannauer, M., Arifin, A. J., and Heinrichs, D. E. (2015) Involvement of reductases IruO and NtrA in
5 iron acquisition by *Staphylococcus aureus*. *Mol. Microbiol.* *96*, 1192-1210.
- 6 (22) Finn, R. D., Bateman, A., Clements, J., Coghill, P., Eberhardt, R. Y., Eddy, S. R., Heger, A.,
7 Hetherington, K., Holm, L., Mistry, J., Sonnhammer, E. L., Tate, J., and Punta, M. (2014) Pfam: the
8 protein families database. *Nucleic Acids Res.* *42*, D222-230.
- 9 (23) Krissinel, E., and Henrick, K. (2007) Inference of macromolecular assemblies from crystalline state. *J.*
10 *Mol. Biol.* *372*, 774-797.
- 11 (24) Oprian, D. D., and Coon, M. J. (1982) Oxidation-reduction states of Fmn and Fad in NADPH-
12 cytochrome P-450 reductase during reduction by NADPH. *J. Biol. Chem.* *257*, 8935-8944.
- 13 (25) Voss, N. R., and Gerstein, M. (2010) 3V: cavity, channel and cleft volume calculator and extractor.
14 *Nucleic Acids Res.* *38*, W555-562.
- 15 (26) Glaser, P., Frangeul, L., Buchrieser, C., Rusniok, C., Amend, A., Baquero, F., Berche, P., Bloecker, H.,
16 Brandt, P., Chakraborty, T., Charbit, A., Chetouani, F., Couve, E., de Daruvar, A., Dehoux, P.,
17 Domann, E., Dominguez-Bernal, G., Duchaud, E., Durant, L., Dussurget, O., Entian, K. D., Fsihi, H.,
18 Garcia-del Portillo, F., Garrido, P., Gautier, L., Goebel, W., Gomez-Lopez, N., Hain, T., Hauf, J.,
19 Jackson, D., Jones, L. M., Kaerst, U., Kreft, J., Kuhn, M., Kunst, F., Kurapkat, G., Madueno, E.,
20 Maitournam, A., Vicente, J. M., Ng, E., Nedjari, H., Nordsiek, G., Novella, S., de Pablos, B., Perez-
21 Diaz, J. C., Purcell, R., Rimmel, B., Rose, M., Schlueter, T., Simoes, N., Tierrez, A., Vazquez-
22 Boland, J. A., Voss, H., Wehland, J., and Cossart, P. (2001) Comparative genomics of *Listeria*
23 species. *Science* *294*, 849-852.
- 24 (27) Sheldon, J. R., Marolda, C. L., and Heinrichs, D. E. (2014) TCA cycle activity in *Staphylococcus aureus*
25 is essential for iron-regulated synthesis of staphyloferrin A, but not staphyloferrin B: the benefit
26 of a second citrate synthase. *Mol. Microbiol.* *92*, 824-839.
- 27 (28) Gomez-Gallego, M., Pellico, D., Ramirez-Lopez, P., Mancheno, M. J., Romano, S., de la Torre, M. C.,
28 and Sierra, M. A. (2005) Understanding of the mode of action of Fe(III)-EDDHA as iron chlorosis
29 corrector based on its photochemical and redox behavior. *Chemistry* *11*, 5997-6005.
- 30 (29) Komori, H., Seo, D., Sakurai, T., and Higuchi, Y. (2010) Crystal structure analysis of *Bacillus subtilis*
31 ferredoxin-NADP(+) oxidoreductase and the structural basis for its substrate selectivity. *Protein*
32 *Sci.* *19*, 2279-2290.
- 33 (30) Muraki, N., Seo, D., Shiba, T., Sakurai, T., and Kurisu, G. (2010) Asymmetric dimeric structure of
34 ferredoxin-NAD(P)+ oxidoreductase from the green sulfur bacterium *Chlorobaculum tepidum*:
35 implications for binding ferredoxin and NADP+. *J. Mol. Biol.* *401*, 403-414.
- 36 (31) Holm, L., and Rosenstrom, P. (2010) Dali server: conservation mapping in 3D. *Nucleic Acids Res.* *38*,
37 W545-W549.
- 38 (32) Williams, C. H., Jr. (1995) Mechanism and structure of thioredoxin reductase from *Escherichia coli*.
39 *FASEB J.* *9*, 1267-1276.
- 40 (33) Trott, O., and Olson, A. J. (2010) AutoDock Vina: improving the speed and accuracy of docking with
41 a new scoring function, efficient optimization, and multithreading. *J. Comput. Chem.* *31*, 455-
42 461.
- 43 (34) Richardson, A. R., Dunman, P. M., and Fang, F. C. (2006) The nitrosative stress response of
44 *Staphylococcus aureus* is required for resistance to innate immunity. *Mol. Microbiol.* *61*, 927-
45 939.
- 46 (35) Nobre, L. S., and Saraiva, L. M. (2013) Effect of combined oxidative and nitrosative stresses on
47 *Staphylococcus aureus* transcriptome. *Appl. Microbiol. Biotechnol.* *97*, 2563-2573.
- 48 (36) Zheng, M., Wang, X., Doan, B., Lewis, K. A., Schneider, T. D., and Storz, G. (2001) Computation-
49 directed identification of OxyR DNA binding sites in *Escherichia coli*. *J. Bacteriol.* *183*, 4571-4579.
- 50 (37) Zheng, M., Aslund, F., and Storz, G. (1998) Activation of the OxyR transcription factor by reversible
51 disulfide bond formation. *Science* *279*, 1718-1721.
- 52
53
54
55
56
57
58
59
60

- 1
2
3 (38) Vanduyne, G. D., Standaert, R. F., Karplus, P. A., Schreiber, S. L., and Clardy, J. (1993) Atomic
4 structures of the human immunophilin FKBP-12 complexes with FK506 and rapamycin. *J. Mol.*
5 *Biol.* 229, 105-124.
6
7 (39) Kabsch, W. (2010) XDS. *Acta Crystallogr. D* 66, 125-132.
8 (40) Adams, P. D., Afonine, P. V., Bunkoczi, G., Chen, V. B., Davis, I. W., Echols, N., Headd, J. J., Hung, L.
9 W., Kapral, G. J., Grosse-Kunstleve, R. W., McCoy, A. J., Moriarty, N. W., Oeffner, R., Read, R. J.,
10 Richardson, D. C., Richardson, J. S., Terwilliger, T. C., and Zwart, P. H. (2010) PHENIX: a
11 comprehensive Python-based system for macromolecular structure solution. *Acta Crystallogr. D*
12 66, 213-221.
13 (41) Emsley, P., Lohkamp, B., Scott, W. G., and Cowtan, K. (2010) Features and development of Coot.
14 *Acta Crystallogr. D* 66, 486-501.
15 (42) Battye, T. G., Kontogiannis, L., Johnson, O., Powell, H. R., and Leslie, A. G. (2011) iMOSFLM: a new
16 graphical interface for diffraction-image processing with MOSFLM. *Acta Crystallogr. D* 67, 271-
17 281.
18 (43) Evans, P. R. (2011) An introduction to data reduction: space-group determination, scaling and
19 intensity statistics. *Acta Crystallogr. D* 67, 282-292.
20 (44) Riener, C. K., Kada, G., and Gruber, H. J. (2002) Quick measurement of protein sulfhydryls with
21 Ellman's reagent and with 4,4'-dithiodipyridine. *Anal. Bioanal. Chem.* 373, 266-276.
22 (45) Stookey, L. L. (1970) Ferrozine - a new spectrophotometric reagent for iron. *Anal. Chem.* 42, 779-
23 781.
24 (46) Lee, W. C., Reniere, M. L., Skaar, E. P., and Murphy, M. E. P. (2008) Ruffling of metalloporphyrins
25 bound to IsdG and IsdI, two heme-degrading enzymes in *Staphylococcus aureus*. *J. Biol. Chem.*
26 283, 30957-30963.
27 (47) Skaar, E. P., Gaspar, A. H., and Schneewind, O. (2004) IsdG and IsdI, heme-degrading enzymes in the
28 cytoplasm of *Staphylococcus aureus*. *J. Biol. Chem.* 279, 436-443.
29
30
31
32
33
34
35
36
37
38
39
40
41
42
43
44
45
46
47
48
49
50
51
52
53
54
55
56
57
58
59
60

1
2
3 **Tables**
4
5

6 **Table 1.** Steady-state kinetic constants for rdIruO and oxIruO.
7

8
9

Kinetic Parameter	Fe(III)-DFB		Fe(III)-FCA	
	rdIruO	oxIruO	rdIruO	oxIruO
<i>Varying siderophore</i>				
K_m (μM)	25 ± 3	28 ± 4	22 ± 4	108 ± 14
k_{cat} (s^{-1})	0.082 ± 0.003	0.018 ± 0.007	0.15 ± 0.006	0.084 ± 0.005
k_{cat}/K_m ($\text{M}^{-1}\text{s}^{-1}$)	3300	660	6700	780
<i>Varying NADPH</i>				
K_m (μM)	44 ± 8	12 ± 1	66 ± 25	61 ± 10
k_{cat} (s^{-1})	0.045 ± 0.005	0.011 ± 0.001	0.11 ± 0.02	0.13 ± 0.01
k_{cat}/K_m ($\text{M}^{-1}\text{s}^{-1}$)	1000	950	1700	2100

10
11
12
13
14
15
16
17
18
19
20
21
22
23
24
25
26
27
28
29
30
31
32
33
34
35
36
37
38
39
40
41
42
43
44
45
46
47
48
49
50
51
52
53
54
55
56
57
58
59
60

Figure Legends

Figure 1. IruO reduces Fe(III)-hydroxamate-type siderophores. rdIruO catalyzed the reduction and release of Fe(II) from (A) 100 μM Fe(III)-DFB (desferrioxamine B), (B) 100 μM Fe(III)-FCA (ferrichrome A), but not (C) 100 μM Fe(III)-EDDHA. An increase in absorbance at 562 nm indicated formation of a Fe(II)-ferrozine complex. The spectra were recorded every 30 seconds for 10 minutes. The red and blue lines indicate the initial and final spectra, respectively. The buffer was 50 mM sodium phosphate, pH 7.4. The structures of the corresponding siderophore structures are drawn with the Fe(III) coordinating atoms in red.

Figure 2. Structure of IruO. (A) Overall fold of rdIruO with the backbone shown as a cartoon diagram. rdIruO is composed of two domains (NADPH, PNDO), a hinge region and a C-terminal α -helix. (B) The rdIruO dimer constructed from crystallographic symmetry. Individual rdIruO subunits are colored gold and teal. (C) The FAD binding site in the PNDO domain. Selected residues interacting with the cofactor are shown as sticks and water molecules as small blue spheres. The oxygen and nitrogen atoms are colored red and blue, respectively. The dashed lines represent hydrogen bonds. (D) The rdIruO dimer is shown as a surface representation and the glycerol (GOL) and FAD molecules are shown as sticks with carbon atoms colored magenta and blue, respectively. Regions of the surface contributed by the NADPH and PNDO domains are labelled as well as residues of the hinge region and C-terminal α -helix.

Figure 3. IruO reduces Fe(III)-DFB using NADPH via FAD. (A) UV-visible absorption spectra of 30 μM rdIruO (FAD_{ox}). UV-visible absorption spectra of 30 μM rdIruO after the addition of (B) 20 μM NADPH and (C) 100 μM sodium dithionite. Initial spectra are in red, spectra in black were recorded every 30 s for 5 min. and the final spectra are in blue. The green line in (C) represented the spectra observed immediately after the addition of sodium dithionite. (D) NADPH titration experiment against 30 μM rdIruO FAD_{ox} recorded at 600 nm. The intersection between the blue and red lines indicates the concentration of NADPH necessary to fully reduce FAD_{ox} (0.5:1 molar ratio of NADPH to IruO subunit). (E) UV-visible absorption spectra of 30 μM rdIruO, pre-incubated with 20 μM NADPH, followed by the addition of (E) 60 μM Fe(III)-DFB and (F) 60 μM Ga(III)-DFB. Spectra were recorded every 30 s for 5 min. Red and blue lines indicate the initial and final spectra, respectively. The arrows indicate the direction of spectral changes over time. The buffer was 50 mM sodium phosphate, pH 7.4.

Figure 4. OxIruO contains an intramolecular disulfide bond. (A) An overlay between rdIruO (gold) and oxIruO (dark grey). Both forms of IruO are shown as a cartoon diagram and the FAD cofactors are shown as sticks. (B) Top-down view of the NADPH domain of oxIruO overlaid with rdIruO. (C) A close up view of the FAD binding site reveals the conformational changes adopted by Cys248 and Cys265 upon oxidation. Cysteine residues and FAD molecules are shown as sticks. The FAD is colored dark blue and light blue for rdIruO and oxIruO, respectively. The dashed lines indicate the distance between the C α atoms of Cys248 and Cys265 in rdIruO and oxIruO. (D) The oxIruO dimer around the FAD cofactor is shown as a surface representation with the subunits colored grey and light blue. The FAD is colored turquoise and shown as sticks. Oxygen, nitrogen and sulfur atoms are colored red, blue and yellow, respectively. Regions of the surface contributed by the NADPH and PNDO domains are labelled as well as residues of the hinge region and C-terminal α -helix.

1
2
3
4
5
6 **Scheme 1. Proposed mechanism for Fe(III)-siderophore reduction via IruO.** FADH*
7 represents FAD in the semiquinone state.
8
9
10
11
12
13
14
15
16
17
18
19
20
21
22
23
24
25
26
27
28
29
30
31
32
33
34
35
36
37
38
39
40
41
42
43
44
45
46
47
48
49
50
51
52
53
54
55
56
57
58
59
60

Figures

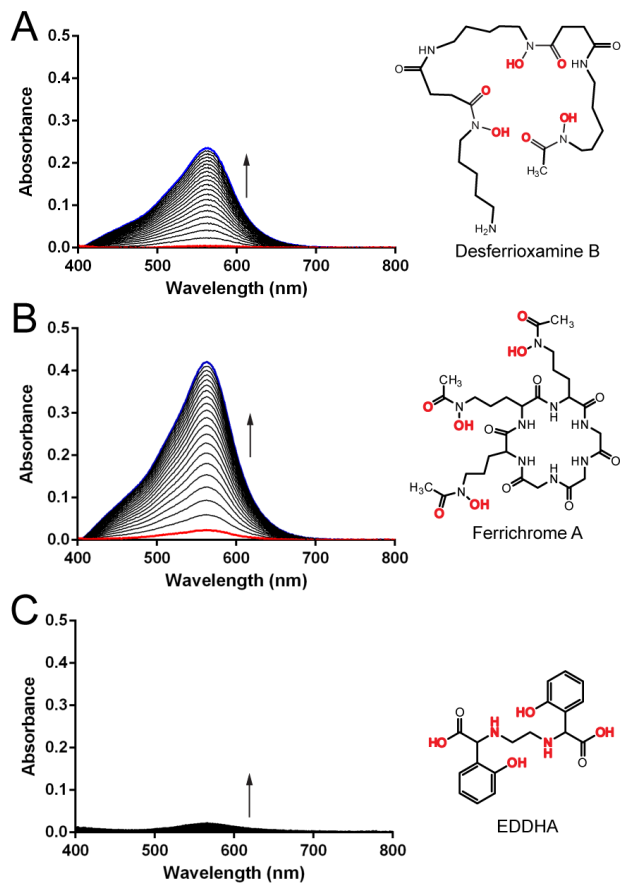


Figure 1.

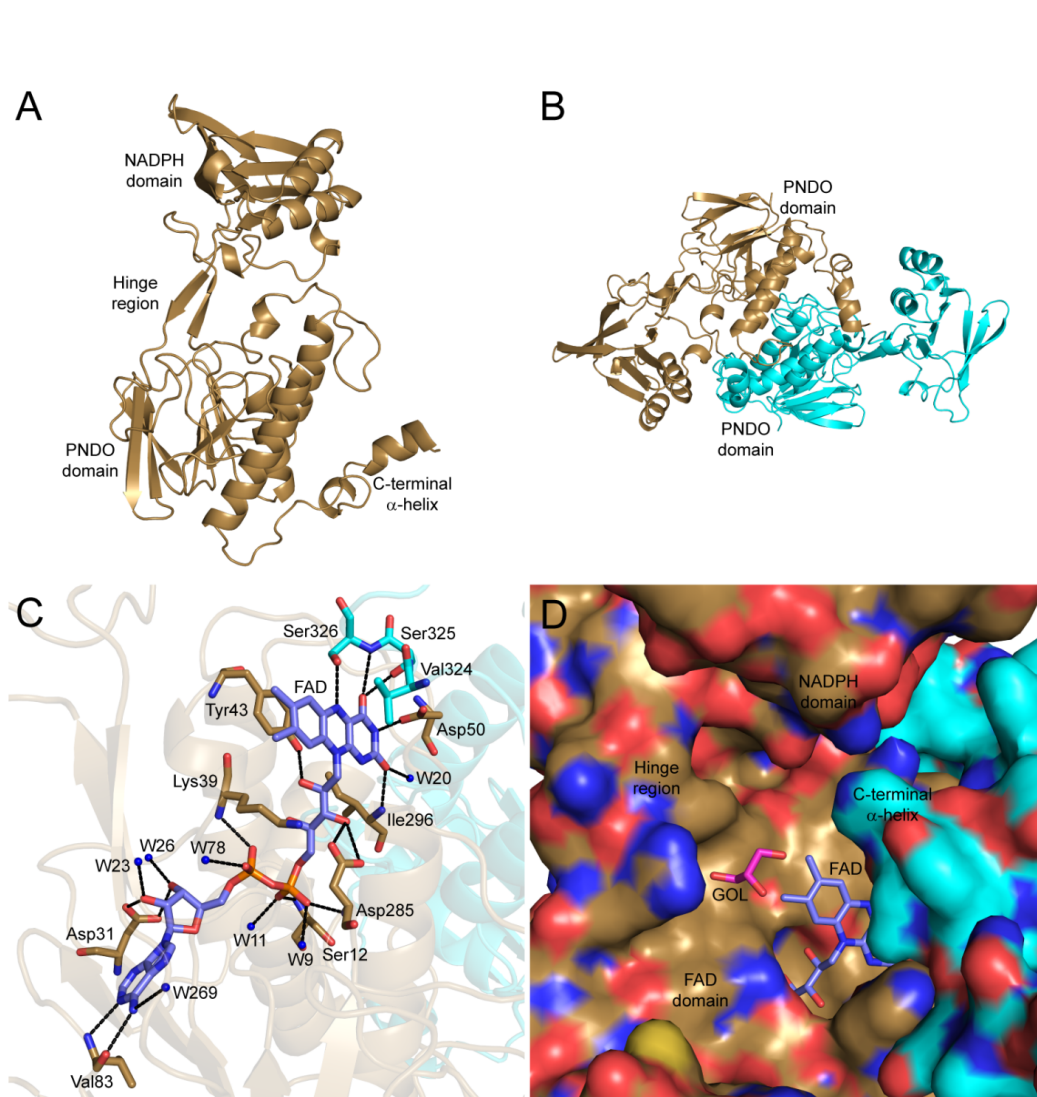


Figure 2

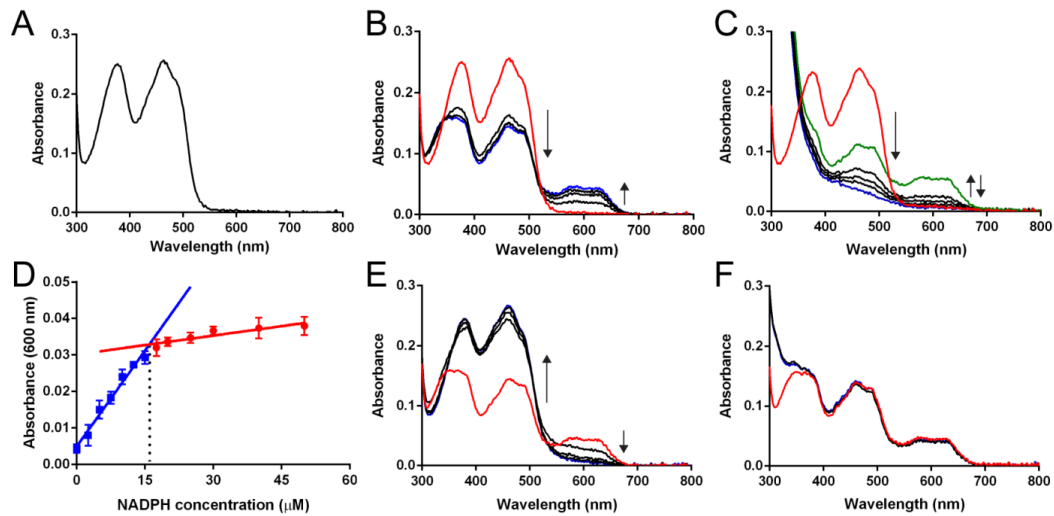


Figure 3

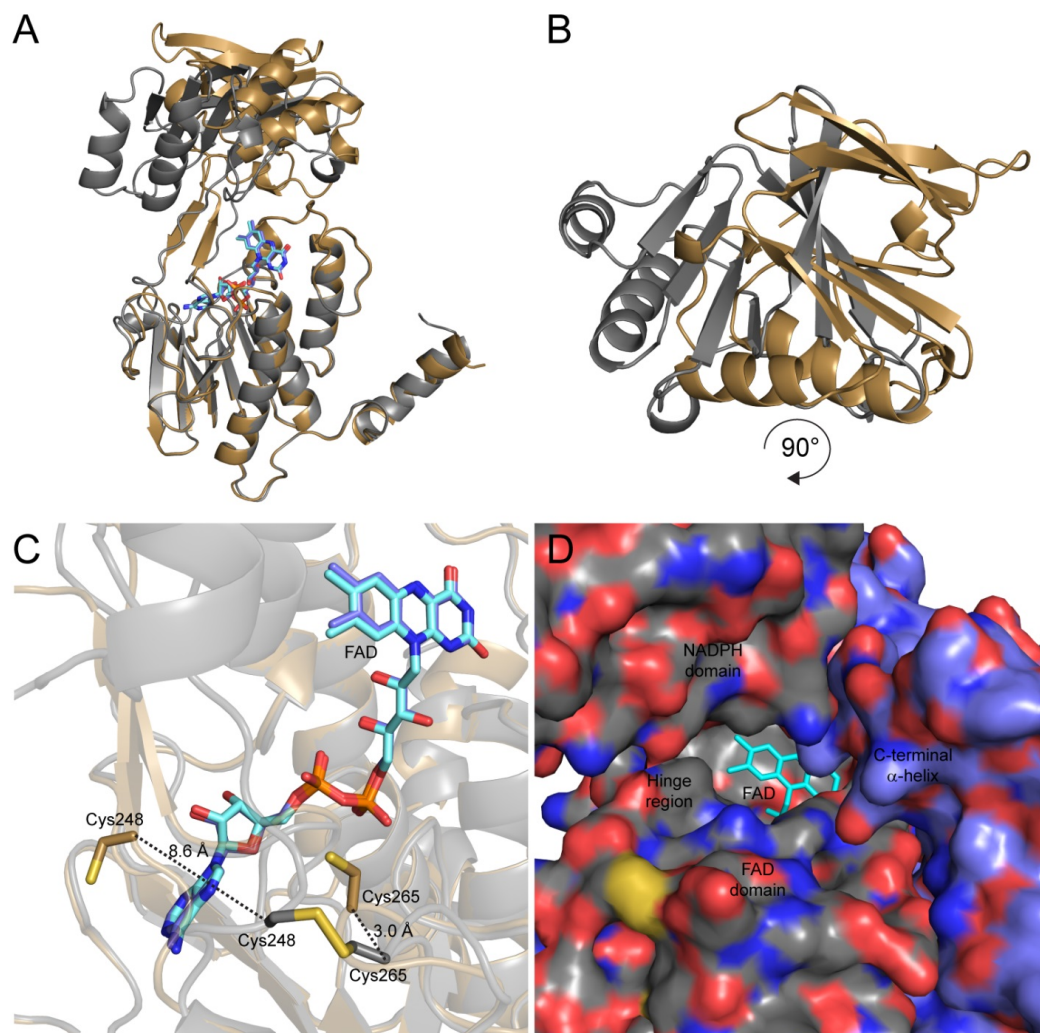
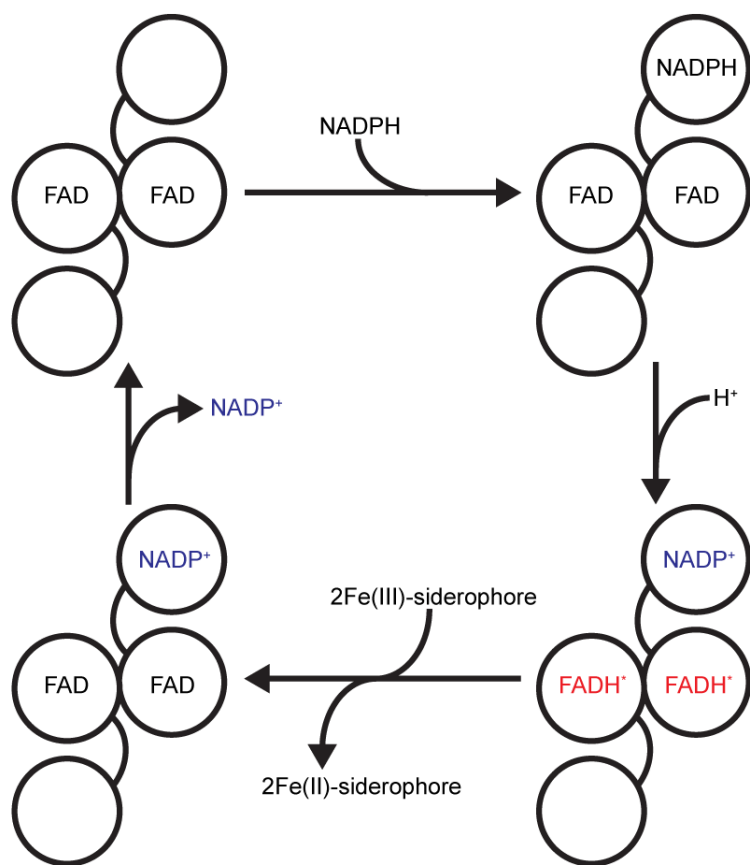
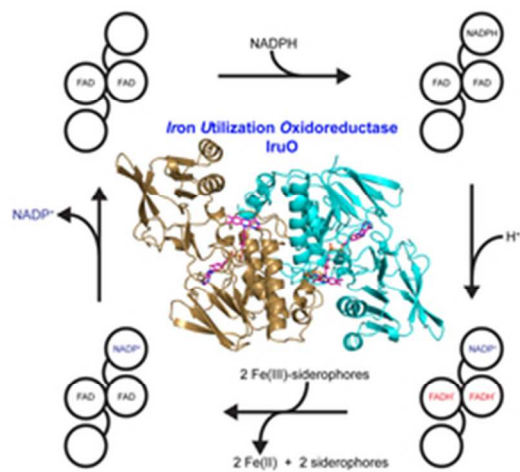


Figure 4



Scheme 1.



Graphic for TOC

39x19mm (300 x 300 DPI)